TUMOR PROGRESSION AND PHARMACOLOGICAL INTERVENTION: MODELING IMMUNOTHERAPEUTIC AND CHEMOTHERAPY STRATEGIES IN NEUROBLASTOMA

Kate Brockman[2], Brian Colburn[1], Joseph Garza[3], Yidong Liao[1], and BV Shankara Narayana Rao[1]

[1]Department of Mathematics and Statistics, Texas A&M University - Corpus Christi
[2]Department of Engineering, Texas A&M University - Corpus Christi
[3]Department of Life Sciences, Texas A&M University - Corpus Christi

Abstract. Neuroblastoma, one of the most common solid tumors found in children is one of the leading causes of childhood cancer. Despite advancements in treatment, there is still an ongoing need for optimal therapy strategies and more accurate mathematical models to guide clinical decision-making for neuroblastoma patients. Among available treatments, immunotherapy and chemotherapy, particularly the use of Interleukin-2 (IL-2) and Cyclophosphamide, have shown encouraging results by enhancing the immune-response and targeting cancerous cells. Therefore, in this study we developed a nonlinear system of coupled first-order differential equations to simulate the interactions between tumor cells, natural killer (NK) cells, and cytotoxic T lymphocytes (CTLs). The model accounted for the effects of IL-2 and Cyclophosphamide on these immune cell populations, by examining tumor dynamics across different patient risk groups. The resulting framework provides a theoretical approach for optimizing therapeutic strategies and improving clinical outcomes in neuroblastoma treatment.

1. Introduction. Cancer is characterized as a disease associated by the uncontrolled proliferation of abnormal cells. These cells invade and disrupt surrounding healthy tissue and have been proven to be caused by a combination of genetic predispositions, environmental exposures, or lifestyle-related factors [20]. Neuroblastoma, holds a significant place in pediatric oncology due to its high prevalence in children with early development occurring most commonly in infants within their first year of life, which may present as either localized or widespread metastatic disease [21]. It accounts for approximately 8% of all childhood cancers and 15% of childhood cancer-related mortality [21]. Overall, the rate at which neuroblastoma is cured can surpass 90%, with 5-year survival rates for low to moderate-risk patients extending from 95% to 100%, and high-risk from 45% to 50% [7]. Clinically, patients are classified into various risk categories outlined by the International Neuroblastoma Risk Group (INRG). For this study, we stratified patient populations into three groups: low risk, intermediate risk, and high risk, based on an existing framework shown in Table 3, which takes into account factors such as age, tumor stage, histology, and genetic components. For low-risk patients, the tumor is regional meaning it is confined to one body compartment [1]. These patients have an estimated survival rate above 98%; observation or surgical resection is usually sufficient for tumor redaction. Intermediate-risk patients are defined as ipsilateral, which means that both the left and right sides of the body are involved [13]. These patients have a survival rate exceeding 90%, and receive chemotherapy in combination with surgery. In contrast, high-risk patients undergo a multi-faceted approach that includes multiple cycles of chemotherapy, surgical resection, radiation and immunotherapy [2]. High risk patients are categorized by a top and or bottom regional tumor with enlarged lymph nodes, particularly in patients less than 18 months of age [13]. This standardized risk-differentiated patient classification system facilitates better survival outcomes by providing an objective framework to optimize treatment strategies in neuroblastoma, whilst minimizing long-term adverse effects of treatment. Given the increasing use of immunotherapies in treatment regimens, a deeper understanding of the immune system's role in tumor control has now become essential [1].

Biologically, the immune response in humans can be broken up into a two-part system: the innate and adaptive immune systems; each contributing uniquely to tumor recognition and elimination [8]. NK cells are often modeled in association with the innate immune system, representing rapid and non-specific responses to cancerous cells, while CTLs, in contrast, are associated with the adaptive immune system with cells that assemble antigen-specific responses following activation [11]. The differentiation is central to the development of any immunotherapeutic framework, as it reflects the differences in cell activation timing and therapeutic targeting in human bodies. By incorporating both NK cells and CTLs into the pharmacological models described in the literature, the complementary roles of innate and adaptive immunity are effectively captured, offering deeper insight into tumor–immune interactions under diverse therapeutic conditions [18]. These distinctions serve as the basis for developing models that simulate immune responses across diverse patient populations and treatment regimens.

Treatment of neuroblastoma has often involved a combination of both chemotherapy and immunotherapeutic agents. In particular, Cyclophosphamide, representing the chemotherapy drug carries cytotoxic activity that directly targets tumor cells by killing them, whilst Interleukin-2 (IL-2), representing the immunotherapeutic approach, stimulates the generation of NK cells. Cyclophosphamide acts to reduce tumor cell populations by inducing apoptosis, thereby decreasing overall tumor burden [12]. Concurrently, IL-2 enhances the immune response by increasing NK cell proliferation rates, bolstering innate immune capabilities against tumor progression. These two drugs are often used in cancer treatment, including neuroblastoma, to slow down the spread of cancer while allowing other treatments such as surgery, radiation, or immunotherapy to take effect [5].

Historically, mathematical modeling has played an important role in cancer research, bridging the gap be-

tween theoretical biology and clinical applications [3, 4, 10, 14, 15, 17, 22]. As our collective biological understanding of cancer has increased, mathematical and computational models have become essential tools for integrating diverse data types and biological processes into frameworks capable of simulating the treatment outcomes of cancer patients [17]. In the context of neuroblastoma, models such as the one developed, offer valuable insights into tumor progression, therapeutic response, and theoretical disease evolution. They support a wide range of applications, including the optimization of chemotherapy scheduling, immunotherapy planning, and personalized treatment strategies [9]. Furthermore, mathematical models enable the formulation of testable hypotheses and the incorporation of experimental and clinical data into predictive simulations [17]. However, despite their promise, oncological modeling is challenged by the inherent complexity of biological systems and the rigorous demands of model validation, verification, and clinical integration [9].

2. Model. Model selection involved testing reported frameworks and parameters from published peer reviewed studies. The described growth models below were among the most commonly cited in available tumor modeling literature [3, 4, 10, 14, 15, 17, 22]:

$$\text{Exponential Growth:} \quad \frac{dT}{dt} = rT \tag{2.1}$$

The exponential model for tumor growth assumes that cells divide at a fixed rate, with a constant cell cycle duration, resulting in exponential expansion. The same growth pattern holds in extended scenarios where either a consistent proportion of the tumor volume is actively proliferating or where cell cycle durations vary randomly but follow an exponential distribution, provided that individual cell cycle lengths are independent and identically distributed [4].

$$\text{Logistic Growth:} \quad \frac{dT}{dt} = rT\left(1 - \frac{T}{K}\right) \tag{2.2}$$

The logistic model describes tumor growth as a process where the relative growth rate $\frac{dT}{dt}$ decreases linearly, with r acting as a parameter linked to proliferation. The framework can be viewed as cells competing for limited resources like nutrients or space. Under this model, the probability of a cell proliferating at any given moment in time is proportional to $1 - \frac{T}{K}$. The logistic model has been widely applied to biological systems to characterize tumor growth, capturing dynamics at both the macroscopic and microscopic scales [4].

$$\text{Gompertz Growth:} \quad \frac{dT}{dt} = rT\ln\left(\frac{K}{T}\right) \tag{2.3}$$

The Gompertz model incorporates the coefficient r representing the initial rate of cell proliferation. The model has gained broad recognition as a fundamental framework for describing growth dynamics, particularly in tumor development. Notablly, a defining feature of the Gompertz model is its characteristic exponential decline in the relative growth rate over time [4].

$$\text{von Bertalanffy Growth:} \quad \frac{dT}{dt} = pT^m - qT^n \tag{2.4}$$

Von Bertalanffy, later followed by other researchers, aimed to establish general principles of organic growth based on fundamental energetics. Benzekry proposed that net growth arises from the balance between organic synthesis and degradation, noting that metabolic rates frequently adhere to the allometric law where they scale with a power of total size and assuming that catabolic rates are proportional to overall volume [4]. This work provided expressions for key coefficients are in terms of measurable energetic quantities [4].

$$\text{Power Law Growth:} \quad \frac{dT}{dt} = rT^p \tag{2.5}$$

The power law model builds on previous reasoning by asserting that in tumor growth, the synthesis rate of new tissue is proportional to the number of proliferating cells, assuming a constant cell cycle duration. This leads

to the conclusion that the proliferative tissue scales with T. When the exponent p falls within the range $0 < p < 1$, tumors exhibits a declining growth fraction and progressively slower relative growth rate. The power law framework captures these dynamics through geometrical interpretations of proliferative tissue. Initially, this model was applied to describe tumor growth in murine studies [4].

Model selection for this study involved testing reported frameworks and parameters, with subsequent customization to assess the feasibility of simulating tumor growth under pharmacological treatments. Iterations of constants were repeated to develop the best-represented model to predict neuroblastoma tumor progression. Stability analyzes and fractional-order modeling using Caputo derivatives was performed on a nondimensionalized system to further refine behavior and enhance model cohesion.

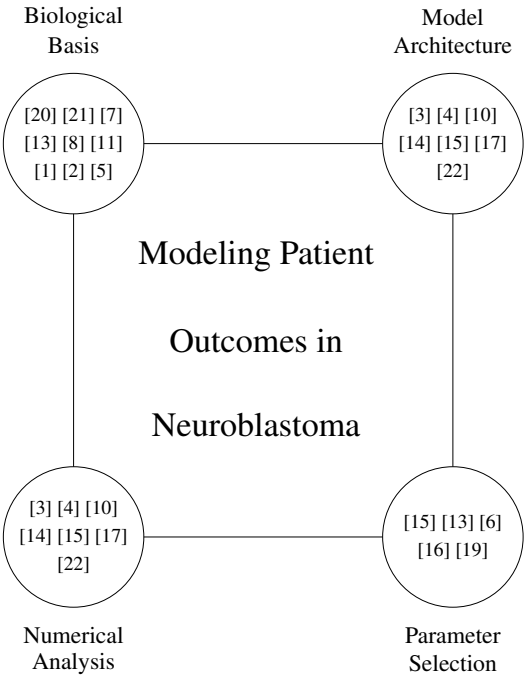

Fig. 1: Tumor-pharmacology model formulation.

2.1. Tumor-pharmacology model. The developed Tumor-pharmacology model builds on a coupled ODE-based framework by Song [23], which describes the dynamic interactions between tumor cells, NK cells, and CTLs under the assumption that cell populations followed a symmetric distribution. Although Song's model captured baseline immune surveillance, it did not account for pharmacological interventions or disease-specific mechanisms relevant to the proposed neuroblastoma therapy.

The developed framework in this study integrates five critical biological and pharmacological components: NK cells, CTLs, tumor cells, IL-2 immunotherapy, and Cyclophosphamide chemotherapy. The system captures complex time-based dynamics of tumor-immune interactions under therapeutic interventions. The model provides a tool for predicting treatment outcomes across various patient populations commonly denoted in the treatment of neuroblastoma patients. The model represents both the direct cytotoxic effects of immune cells and drugs, as well as the indirect immunostimulation effects that shape the tumor microenvironment.

$$
\begin{cases}
N'(t) = a_1 N(t)(1 - bN(t)) - a_2 N(t) - \alpha_1 N(t)T(t) + k_i I(t) \\
L'(t) = r_1 N(t)T(t) - \mu L(t) - \beta_1 L(t)T(t) \\
T'(t) = cT(t)(1 - dT(t)) - \alpha_2 N(t)T(t) - \beta_2 L(t)T(t) - k_c C(t) \\
I'(t) = -\dfrac{\log(2)}{h_i} 2^{-\frac{t}{h_i}} I(0) \\
C'(t) = -\dfrac{\log(2)}{h_c} 2^{-\frac{t}{h_c}} C(0)
\end{cases}
\tag{2.6}
$$

Parameters for the Tumor-pharmacology model are shown in Table 1.

Table 1: Tumor-pharmacology model parameters.

Parameter	Description	Units
a_1	NK cell growth rate	cell $\cdot$ day^{-1}
a_2	NK cell death rate due to natural death	day^{-1}
b	Carrying capacity coefficient for NK cell population	cell^{-1}
c	Natural tumor cell growth rate	day^{-1}
d	Carrying capacity coefficient for tumor cell population	cell^{-1}
α_1	Rate of NK cell death due to tumor interaction	cell^{-1} $\cdot$ day^{-1}
α_2	Rate of NK-induced tumor death	cell^{-1} $\cdot$ day^{-1}
β_1	Rate of CTL-cell death due to tumor interaction	cell^{-1} $\cdot$ day^{-1}
β_2	Rate of CTL-induced tumor death	cell^{-1} $\cdot$ day^{-1}
μ	CTL cell death rate due to natural death	day^{-1}
r_1	Rate of NK-lysed tumor cell debris activation of CTLs	cell^{-1} $\cdot$ day^{-1}
k_c	Rate constant of Cyclophosphamide-mediated tumor death	mg^{-1} $\cdot$ day^{-1} $\cdot$ cell
k_i	Rate constant of IL-2-mediated stimulation	IU^{-1} $\cdot$ day^{-1} $\cdot$ cell
h_i	Half-life of IL-2	min
h_c	Half-life of Cyclophosphamide	min
I_0	Dose of IL-2	IU
C_0	Dose of Cyclophosphamide	mg

2.1.1. Cellular Dynamics. In this model, $N(t)$, $L(t)$, and $T(t)$ denote the populations of NK cells, CTLs, and neuroblastoma tumor cells, respectively.

The NK cell dynamics incorporate four key mechanisms: (1) Logistic proliferation with intrinsic growth rate a_1 and carrying capacity $1/b$, capturing growth constraints; (2) Natural death at rate a_2, reflecting cell turnover; (3) Tumor-induced depletion through interactions with tumor cells, modeled by $-\alpha_1 NT$; (4) IL-2-stimulated recruitment represented by $k_i I$, which captures the immunostimulatory effects of IL-2 therapy. The parameter k_i quantifies the pharmacological efficacy of IL-2 per unit concentration.

The CTL population evolves based on three principal processes: (1) Activation via NK–tumor interactions, described by $r_1 NT$, where r_1 characterizes the rate of CTL recruitment in response to tumor-derived signals; (2) Natural decay at rate $-\mu L$; (3) Functional exhaustion during sustained tumor engagement, represented by $-\beta_1 LT$.

The tumor cell population is governed by four biological mechanisms: (1) Logistic growth $cT(1 - dT)$ with intrinsic growth rate c and carrying capacity $1/d$; (2) NK cell-mediated cytotoxicity $-\alpha_2 NT$; (3) CTL-driven antigen-specific killing $-\beta_2 LT$; (4) Chemotherapy-induced death $-k_c C$, reflecting the dose-dependent effect of Cyclophosphamide. Parameters α_2 and β_2 quantify the cytotoxic effectiveness of NK and CTL cells, respectively, while k_c denotes the potency of the applied chemotherapeutic treatment.

2.1.2. Pharmacology Dynamics. In this model, the variables $I(t)$ and $C(t)$ represent the concentrations of IL-2 and Cyclophosphamide. Both follow first-order exponential decay, a standard method for modeling drug elimination. The decay rates are governed by the agents half-lives h_i and h_c, with terms $\frac{\log(2)}{h_i}$ and $\frac{\log(2)}{h_c}$ ensuring that each drug concentration decreases by half over its respective half-life interval. Initial conditions $I(0)$ and $C(0)$ correspond to the administered doses at $t = 0$.

Both of the selected drugs actively have an effect on biological systems. IL-2 enhances NK cell activity through the stimulatory term $k_i I(t)$ in the NK cell equation $N'(t)$, promoting immune activation. Conversely, Cyclophosphamide contributes to tumor reduction via the cytotoxic term $-k_c C(t)$ in the tumor cell equation $T'(t)$. Both of these two interactions highlight the dual role of pharmacokinetics: while drug concentrations diminish over time, their time-based presence significantly shapes tumor–immune dynamics through modulation of cell behavior.

2.2. Nondimensionalization. To reduce model complexity and highlight biological mechanisms, the system was rewritten in a nondimensionalized form, using appropriate scaling transformations based on characteristic population sizes and rates. The number of parameters in the system was reduced from 17 to 13 after nondimensionalization. This approach reformulated the equations regarding dimensionless variables and parameters, allowing for a straightforward interpretation and comparison across treatment groups.

$$
\begin{cases}
N'(t) = p_1 N(t)(1 - qN(t)) - p_2 N(t) - N(t)T(t) + k_i I(t) \\
L'(t) = N(t)T(t) + rD(t) - L(t) - sL(t)T(t) \\
T'(t) = uT(t)(1 - vT(t)) - N(t)T(t) - \delta L(t)T(t) - k_c C(t) \\
I'(t) = -\dfrac{\log(2)}{h_i} 2^{-\frac{t}{h_i}} I(0) \\
C'(t) = -\dfrac{\log(2)}{h_c} 2^{-\frac{t}{h_c}} C(0)
\end{cases} \tag{2.7}
$$

The simplification brings about parameters $p_1 = \frac{a_1}{\mu}$ and $p_2 = \frac{a_2}{\mu}$, which normalize the NK cell proliferation and natural death rates relative to the CTL death rate μ. The parameter $q = \frac{b}{\mu\alpha_2}$ represents the NK cell carrying capacity scaled by the NK-induced tumor cell death rate. The parameter $k_i = \frac{k_i\alpha_2}{\mu^2}$ results in a nondimensionalized dose of IL-2.

The term $r = \frac{T(0)}{\alpha_1\alpha_2} \cdot \frac{r_1}{\mu}$ accounts for CTL activation resulting from tumor cell by-products generated by NK-induced cytotoxicity, scaled by the initial tumor burden. The parameter $s = \frac{\beta_1}{\alpha_1}$ expresses the relative rates at which CTLs and NK cells are lost through interactions with tumor cells.

The tumor growth rate is scaled as $u = \frac{c}{\mu}$, and the term $v = \frac{du}{\alpha_1}$ captures the effects of tumor carrying capacity modulated by NK activity. Finally, $\delta = \frac{\beta_2 r_1}{\alpha_1\alpha_2}$ characterizes the CTL-induced tumor cell death rate relative to that of NK cells and $k_c = \frac{k_c\alpha_1}{\mu^2}$ scales the Cyclophosphamide dose to the growth of NK cells and the death of CTL cells. Together, these nondimensionalized parameters highlight the main mechanisms governing tumor-immune dynamics and enable a more generalized analysis across treatments and patient disease profiles.

2.3. Model Behavior Prediction. The system exhibits three characteristic dynamical regimes based on parameter relationships: tumor elimination, chronic equilibrium, and tumor escape. Each regime reflects a distinct biological outcome driven by the balance between tumor proliferation, immune response, and therapeutic intervention.

2.3.1. Tumor Elimination Regime. Tumor elimination occurs when immune activation and drug efficacy sufficiently overcome tumor growth. The critical condition is achieved when the combined dimensionless killing rates satisfy $\delta + k_c > u(1+v)$. In this state, the tumor population decays exponentially while immune populations stabilize at elevated levels due to persistent antigen stimulation.

2.3.2. Chronic Equilibrium State. Chronic equilibrium states emerges when tumor growth and immune surveillance reach a balance. This requires two conditions: (1) the immune activation ratio $p_1/\delta \approx 1$, indicating balanced NK and CTL contributions, and (2) the drug effect k_c falls within an intermediate range where it modulates but doesn't eliminate the tumor. The system exhibits damped oscillations converging to a fixed point with non-zero tumor burden.

2.3.3. Tumor Escape Phase. Tumor escape phases were characterized by exponential tumor growth, this regime occurs when either (1) the scaled tumor proliferation rate u exceeds the sum of immune efficacy parameters $(p_1+\delta)$, or (2) drug concentrations fall below the critical threshold $k_c < u-\delta$. The model predicts rapid divergence of the tumor population in these parameter regions, corresponding to treatment failure scenarios.

3. Methods. This section outlines the computational and analytical approaches used to model neuroblastoma dynamics and immune response interactions. The Caputo fractional-order derivative is introduced as a means of incorporating memory effects into the system of differential equations governing CTLs, NK cells, and tumor cell populations, as well as proving not only the existence of solution, but a unique solution. By excluding treatment variables (Cyclophosphamide and Interleukin-2), the fractional framework focuses solely on intrinsic immune-tumor interactions across distinct patient-risk categories.

The numerical simulations were executed using Python's SciPy library. Adaptive integration techniques were employed to ensure computational stability and accuracy while tracking tumor progression. The simulations facilitate a comparative analysis of immune responses under varying clinical conditions, providing insight into the effectiveness of fractional-order modeling in capturing tumor evolution.

3.1. Numerical Methods. Numerical simulations were performed in Python using the `SciPy` library. Parameter values that were adapted from existing literature are listed in Table 1, while initial immune and tumor cell counts were determined based on the relative proportions characteristic of each neuroblastoma risk group as discussed previously. Simulations were run across the three patient-risk categories to assess immune response dynamics and treatment effectiveness under the varying clinical conditions with different initial cell populations for each risk category.

3.2. Mathematical Methods. The mathematical method includes the overview of the Caputo fractional order derivative and how it will apply to the tumor model from (2.7).

3.2.1. Caputo Fractional Order Derivative Framework. To enhance the biological nature of our neuroblastoma model, we incorporated a Caputo fractional-order derivative to capture tumor dynamics. This framework applied to three differential equations representing CTL, NK, and Tumor cells, excluding the drug/treatment variables of Cyclophosphamide (C) and Interleukin-2 (IL-2). The Caputo operator will solely focus on the tumor model. This allows the Caputo operator to be applied to equations from (2.7). The Caputo operator facilitated improved accuracy of tumor growth modeling by accounting for past system behavior, as demonstrated in recent studies [10]

Tumor cells, CTLs, and NK cells are denoted by T, L, and N, respectively. All other parameters are defined in Table 1.

Definition 1: Consider the following function $\varphi(t)$, when $t > 0$, and the Riemann-Liouville Integral (RLI) operator of a function $\varphi(t)$ is defined as follows:

$$I^{\alpha}\varphi(t) = \int_0^t \frac{(t-\tau)^{\alpha-1}}{\Gamma(\alpha)}\varphi(\tau)\,d\tau \tag{3.1}$$

where $\alpha > 0$ is the order of integral.

The fractional derivative operator is denoted D_0^{α} and $\alpha > 0$ defines the fractional order allowing to model memory and hereditary effects better than the classical integer order derivatives. $\alpha > 0$ lies between the integer values and the gamma function are the generalization of the factorial function to continuous values, and $(t-\tau)^{\alpha-1}$ is the kernel function that is being integrated and gives the fractional derivative its memory property, where τ is a past time point on the interval $[0, t]$.

The fractional-order derivative of function $\varphi(t)$ in 3.1 is defined by the following:

$$D^{a}\varphi(t) = I^{n-a}D^{(n)}\varphi(t) \tag{3.2}$$

where $D = \frac{d}{dt}$

Definition 2: Consider the function $\varphi(t)$ when $t > 0$, the Caputo fractional derivative of order α when $\alpha > 0$ is given by the following:

$$D^{\alpha}\varphi(t) = \frac{1}{\Gamma(n-\alpha)}\int_0^t (t-\tau)^{n-\alpha-1}\varphi^{(n)}(\tau)\,d\tau \tag{3.3}$$

where n is an integer, and $\alpha \in (n-1, n)$ and $D^{\alpha}\varphi(t)$ is the Caputo fractional operator of the function $\varphi(t)$.

Theorem 1: Consider a system of fractional order equations in the form:

$$D_0^{a}\varphi(t) = \varphi(t, Y(t)), Y(t_0) = Y_0 \tag{3.4}$$

The following statements will be true when J(Y*) is the Jacobian Matrix:

- The equilibrium point is asymptotically stable only if all eigenvalues of the Jacobian Matrix satisfy $0 < q < \frac{1}{u}$ which will be discussed further in 3.2.2
- The equilibrium point is unstable only if all eigenvalues of the Jacobian Matrix such that $p_2 - p_1 > 0$ and $u + \frac{1}{q}(\frac{p_2}{p_1} - 1) > 0$ which will be discussed further in 3.2.2

where p_1, p_2 and $u < 1/q$ or $q < \frac{1}{u}$ are considered saddle points.

Here we generalize an integer-order tumor interaction model, given by the following equations (3.5)–(3.7) is a set that is a continuous nonlinear ordinary differential equation:

$$N'(t) = \alpha_1 N(t)(1 - bN(t)) - \alpha_2 N(t) - \alpha_1 N(t)T(t) \tag{3.5}$$

$$L'(t) = r_1 N(t)T(t) + r_2 D(t) - \mu L(t) - \beta_1 L(t)T(t) \tag{3.6}$$

$$T'(t) = cT(t)(1 - dT(t)) - \alpha_2 N(t)T(t) - \beta_2 L(t)T(t) \tag{3.7}$$

where N, L, and T represent the populations of the natural killer (NK) cells, CTLs, and tumor (T) cells respectively. Furthermore α_1, α_2, b, r_1, r_2, μ, β_1, β_2, and c are all parameters from Table 1.

After non-dimensionalizing equations (3.5)–(3.7), we get the following equations:

$$N'(t) = p_1 N(t)(1 - qN(t)) - p_2 N(t) - N(t)T(t) \tag{3.8}$$

$$L'(t) = N(t)T(t) + rD(t) - L(t) - sL(t)T(t) \tag{3.9}$$

$$T'(t) = uT(t)(1 - vT(t)) - N(t)T(t) - (\delta)L(t)T(t) \tag{3.10}$$

where p_1, p_2, q, r, s, u, v, and δ are the nondimensionalized parameters. Now the proposed dimensionless model is put into Caputo fractional order derivative form with the following equations:

$$D_0^\alpha x(t) = p_1 x(t)(1 - qx(t)) - p_2 x(t)z(t) \tag{3.11}$$

$$D_0^\alpha y(t) = x(t)z(t) + rd(t) - y(t) - sy(t)z(t) \tag{3.12}$$

$$D_0^\alpha z(t) = uz(t)(1 - vz(t)) - x(t)z(t) - \delta y(t)z(t) \tag{3.13}$$

when $\alpha > 0$ is the order derivative, and x(t), y(t), and z(t) represent the respective cell populations of the NK cells, CTLs, and T cells.

In this section, a lemma and definitions will prove the existence of a unique solution of the fractional order tumor model.

Lemma 1: Consider the system of equations defined by Caputo fractional-order derivatives:

$$D^a x(t) = p_1 x(1 - qx) - p_2 xz \tag{3.14}$$

$$D^a y(t) = xz + rd - y - syz \tag{3.15}$$

$$D^a z(t) = uz(1 - vz) - xz - \delta yz \tag{3.16}$$

where $0 < a \leq 1$, and $x(t), y(t)$, and $z(t)$ is simplified even further to x, y, and z respectively. Then the system admits a unique solution under appropriate conditions, ensuring that disturbances in initial conditions do not lead to non-deterministic behaviors. This reinforces the stability of the fractional-order system.

The initial conditions of the fractional order derivatives can be written as $x(t_0) = x_0, y(t_0) = t_0$, and $z(t_0) = z_0$. Equations (3.11)–(3.13) can be written in the form:

$$D^a Y(t) = R_1 Y(t) + x(t)R_2 Y(t), Y(t_0) = Y_0 \tag{3.17}$$

where Y_0 are initial conditions of the function Y(t) which is the column vector of the equations x(t), y(t), and z(t) are the respective population equations of NK cells, CTLs, and tumor cells

$$Y(t) = \begin{bmatrix} x(t) \\ y(t) \\ z(t) \end{bmatrix} \tag{3.18}$$

$$R_1 = \begin{bmatrix} 0 & 0 & 0 \\ 0 & -1 & 0 \\ u & 0 & v \end{bmatrix} \tag{3.19}$$

$$R_2 = \begin{bmatrix} p_1(1-q) & 0 & -p_2 \\ 1 & 0 & 0 \\ -1 & -\delta & -1 \end{bmatrix} \tag{3.20}$$

The following definitions are required for the existence and uniqueness of solutions for equation 3.17.

Definition 3: Consider $C[0,\theta]$ to belong to a continuous vector Y(t) with the components of functions of x(t), y(t), and z(t)

Definition 4: Y(t) is a column vector that satisfies equation (3.20) which belongs to $C[0,\theta]$.

Theorem 2: The system of equations given by equation (3.20) has a unique solution Y(t) that belongs to $C[0,\theta]$

Proof of Lemma 1: The system of fractional order differential equations (3.14)-(3.16) can be written as follows:

$$I^{1-a}\frac{d}{dt}Y(t) = R_1Y(t) + x(t)R_2Y(t) \tag{3.21}$$

where

$$D_\alpha[Y] = I^{1-a}\frac{d}{dt}Y(t) \tag{3.22}$$

$R_1Y(t)$ indicates that Y(t) evolves with a rate proportional to itself (either logistic or exponential growth, or logistic or exponential).

$x(t)R_2Y(t)$ introduces the interaction between y(t) and x(t) indicating that x(t) influences rate of change Y(t). Apply the Riemann-Liouville Integral to operate I^a on both sides of the equation

$$I^a[D_\alpha[Y]] = I^a(R_1Y(t) + x(t)R_2Y(t) \tag{3.23}$$

Here we solve the fractional integral for Y

$$I = \int_o^\tau Y(\tau)d\tau \ = Y(t) - Y(0) \tag{3.24}$$

Substitute Y(t) -Y(0) for I for the integral

$$Y(t) - Y(0) = I^a(R_1Y(t) + x(t)R_2Y(t)) \tag{3.25}$$

Isolate Y(t) to get the initial conditions

$$Y(t) = Y(0) + I^a(R_1Y(t) + x(t)R_2Y(t)) \tag{3.26}$$

Define operator G[Y(t)] which also belongs on the continuous function C[0,θ]

$$G[Y(t)] = Y(0) + I^a(R_1Y(t) + x(t)R_2Y(t)) \tag{3.27}$$

The solution of Y(t) is a fixed point on the operator G, this satisfies certain properties like:

- Mapping into the space: C[0,θ] so that it operates within the continuous function and since Y(0) and $I^\alpha(R_1Y(t) + x(t)R_2Y(t))$ are continuous, the fractional integral I^α preserves continuity
- Contraction mapping: The operator G is a contraction under certain conditions meaning $||G[Y_1(t)] - G[Y_2(t)]|| \leq L||Y_1(t) - Y_2(t)||$, with $L < 1$, which guarantees a unique solution

where I^a represents the Riemann–Liouville fractional integral.

Consider two solutions $Y(t)$ and $Z(t)$ to analyze the difference between two trajectories:

$$G[Y(t)] - G[Z(t)] = I^a[R_1(Y(t) - Z(t)) + R_2(Y(t) - Z(t))] \tag{3.28}$$

Here we introduce the exponential decay factor and multiply both sides of the equation by e^{-nt}:

$$e^{-nt}[G(Y(t)) - G(Z(t))] = e^{-nt}I^a[R_1(Y(t) - Z(t)) + R_2(Y(t) - Z(t))] \tag{3.29}$$

Expand the fractional integral using the definition of the Riemann–Liouville fractional integral to replace I^a:

(3.30)
$$I^a \left[R_1(Y(t) - Z(t)) + R_2(Y(t) - Z(t))\right] = \frac{1}{\Gamma(\alpha)} \int_0^t (t-c)^{\alpha-1} \left[R_1(Y(c) - Z(c)) + R_2(Y(c) - Z(c))\right] dc$$

This formulation ensures that past values $f(c)$ contribute to the present state $f(t)$, weighted by $(t-c)^{a-1}$, which scales historical influence.

Next, apply exponential decay within the integral multiplying by $e^{-n(t-c)}$:

$$\frac{1}{\Gamma(\alpha)} \int_0^t (t-c)^{\alpha-1} e^{-n(t-c)} [Y(c) - Z(c)][R_1 + uR_2]\, dc \tag{3.31}$$

Now introduce norm bound, it ensures that differences between solutions remain controlled over time. Replace the right hand side of (3.28) with (3.30).

$$\|G[Y(t)] - G[Z(t)]\| \leq \frac{1}{\Gamma(\alpha)} \int_0^t (t-c)^{\alpha-1} e^{-n(t-c)} \|Y(t) - Z(t)\| [R_1 + uR_2]\, dc \tag{3.32}$$

Since norm properties allow a unique solution that depends on continuous initial conditions:

$$\|Y(c) - Z(c)\| \leq \|Y(t) - Z(t)\|, \tag{3.33}$$

when applying inequality (3.33) to inequality (3.32), we then factor $\|Y(t) - Z(t)\|$ out of the integral

$$\|G[Y(t)] - G[Z(t)]\| \leq (R_1 + uR_2)\|Y(t) - Z(t)\| \frac{1}{\Gamma(\alpha)} \int_0^t (t-c)^{\alpha-1} e^{-n(t-c)}\, dc \tag{3.34}$$

Now the integral evaluates to $\frac{\Gamma(\alpha)}{n^\alpha}$, we can substitute:

$$\|G[Y(t)] - G[Z(t)]\| \leq (R_1 + uR_2) \frac{1}{n^\alpha} \|Y(t) - Z(t)\| \tag{3.35}$$

so we can conclude:

$$\|G[Y(t)] - G[Z(t)]\| \leq (R_1 + uR_2) \frac{1}{n^\alpha} \|Y(t) - Z(t)\| \int_0^t \frac{\alpha - 1}{\Gamma(\alpha)}\, dc \tag{3.36}$$

This bound ensures stability and controls deviations between trajectories.

Substituting the integral back into our expression because it is the definite integral of a constant independent of c, integrating from $[0, t]$:

$$\|G[Y(t)] - G[Z(t)]\| \leq (R_1 + uR_2) \frac{1}{n^\alpha} \|Y(t) - Z(t)\| \frac{\alpha - 1}{\Gamma(\alpha)} t \tag{3.37}$$

This introduces a bounded scaling factor, which ensures a contraction effect.

Now we establish the contraction property and are observing the structure of the term:

$$\|G[Y(t)] - G[Z(t)]\| \leq (R_1 + uR_2) \frac{t}{n^\alpha \Gamma(\alpha)} \|Y(t) - Z(t)\| \tag{3.38}$$

Since the coefficient $\frac{t}{n^\alpha \Gamma(\alpha)}$ acts as a damping factor, it ensures:

$$\|G[Y(t)] - G[Z(t)]\| < \|Y(t) - Z(t)\| \tag{3.39}$$

The integral term accumulates past influences but remains bounded. The contraction property ensures that the operator G smooths out deviations over time. This proves that G satisfies a stability condition, meaning perturbations diminish rather than grow.

Since the operator $G[Y(t)]$ satisfies a contraction property, we guarantee the existence of a unique fixed solution, meaning:

$$G[Y(t)] = Y(t) \tag{3.40}$$

Thus, $Y(t)$ must satisfy the corresponding integral equation.

Formulation of Solution: Using fractional calculus the Riemann-Liouville Integral, the solution is expressed in terms of the initial condition $Y(0)$ and the fractional integral I^{α}:

$$Y(t) = Y(0) + I^{\alpha}(R_1 Y(t) + x(t) R_2 Y(t)) \tag{3.41}$$

where I^{α} represents memory-dependent contributions.
Expanding the solution form using fractional integral properties:

$$Y(t) = Y(0) + \frac{t^{\alpha}}{\Gamma(\alpha+1)}[R_1 Y(0) + x(0) R_2 Y(0)] + I^{\alpha+1}[R_1 Y'(t) + x'(t) R_2 Y(t) + x(t) R_2 Y'(t)] \tag{3.42}$$

- The first term $Y(0)$ captures the initial state
- The second term introduces memory scaling using Gamma function properties
- The third term accumulates past interactions via the fractional integral $I^{\alpha+1}$, ensuring long-term dependencies

Thus, the existence of a fixed point leads directly to the solution formulation
Operating equation (3.42) to the initial fractional order derivatives stated in equations (3.11)–(3.13):

(3.43)
$$x(t) = x(0) + \frac{t^{\alpha}}{\Gamma(\alpha+1)}[p_1 x(0)(1 - q x(0)) - p_2 x(0) z(0)] + I^{\alpha+1}[p_1(1 - 2q x(t)) x'(t) - p_2(z(t) x'(t) + x(t) z'(t))]$$

(3.44)
$$y(t) = y(0) + \frac{t^{\alpha}}{\Gamma(\alpha+1)}[x(0) z(0) + r d(t) - y(0) - s y(0) z(0)] + I^{\alpha+1}[x'(t) z(t) + x(t) z'(t) - y'(t) - s y'(t) z(t)]$$

$$z(t) = z(0) + \frac{t^{\alpha}}{\Gamma(\alpha+1)}[u(1 - v z(0)) - x(0) z(0) - \delta y(0) z(0)] + I^{\alpha+1}[-v z'(t) - x'(t) z(t) - x(t) z'(t)] \tag{3.45}$$

Each population (N, L, T) now follows fractional-order memory dynamics, meaning past interactions influence current behavior. The Gamma function scaling ensures appropriate historical weighting, while the fractional integral term $I^{\alpha+1}$ allows for persistent effects in tumor-immune interactions. The system accounts for biological delays, making the model more realistic than classical differential equations.

3.2.2. Stability Analysis. Using the nondimensionalized model, we solved for critical points to find $N_0 = L_0 = T_0 = 0$ for the trivial solution, and for non-zero values we have:

$$N_i^* = \frac{p_1 - p_2 \pm \sqrt{4 k_n p_1 q D(t) + p_1^2 - 2 p_1 p_2 - 2 p_1 T(t) + p_2^2 + 2 p_2 T(t) + T^2(t)} - T(t)}{2 p_1 q} \tag{3.46}$$

$$L_i^* = \frac{r D(t) + N(t) T(t)}{s T(t) + 1} \tag{3.47}$$

(3.48)
$$T_i^* = \frac{-\delta L(t) + u \pm \sqrt{\delta^2 L^2(t) - 2\delta u L(t) + 2\delta L(t) N(t) - 4 k_t u v D(t) + u^2 - 2u N(t) + N^2(t)} - N(t)}{2uv}$$

and the Jacobian of the nondimensionalized model is

$$J = \begin{bmatrix} -2p_1qN(t) + p_1 - p_2 - T(t) & 0 & -N(t) & k_n \\ T(t) & -sT(t) - 1 & -sL(t) + N(t) & r \\ -T(t) & -\delta T(t) & -\delta L(t) - 2uvT(t) + u - N(t) & -k_t \\ 0 & 0 & 0 & 0 \end{bmatrix}$$

for the trivial case, the Jacobian becomes

$$J = \begin{bmatrix} p_1 - p_2 & 0 & 0 & k_n \\ 0 & -1 & 0 & r \\ 0 & 0 & u & -k_t \\ 0 & 0 & 0 & 0 \end{bmatrix}$$

This gives us the eigenvalues 0, $p_1 - p_2$, -1, and u. Since u has a positive sign, -1 has a negative sign, and $p_1 - p_2$ could be positive or negative, we can conclude that the trivial case is a saddle point. For the case $L_0 = T_0 = D_0 = 0$, $N_0 = \frac{p_1 - p_2 + \sqrt{p_1^2 - 2p_1p_2 + p_2^2}}{2p_1q} = \frac{1}{q}$

$$J = \begin{bmatrix} -p_1 - p_2 & 0 & -\frac{1}{q} & k_n \\ 0 & -1 & \frac{1}{q} & r \\ 0 & 0 & u - \frac{1}{q} & -k_t \\ 0 & 0 & 0 & 0 \end{bmatrix}$$

This gives us the eigenvalues $-p_1 - p_2$ and -1, which are negative, and $u - \frac{1}{q}$ which could be negative or positive. Since u and q are positive, $u - \frac{1}{q}$ will only be negative when $u < \frac{1}{q}$ or when $q < \frac{1}{u}$. So this set of initial conditions is a saddle point when $q > \frac{1}{u}$ (which corresponds with a NK population cap less than that of the tumor growth rate), and a stable sink when $0 < q < \frac{1}{u}$ (which corresponds with a NK population cap greater than that of the tumor growth rate).

Table 2: Eigenvalue results.

Parameters	Range	Eigenvalue	Stability
p_1	$(0, p_2)$	$p_2 - p_1 > 0$	unstable
p_1	(p_2, ∞)	$p_2 - p_1 < 0$	saddle point
q, p_2	$q \in \left(0, \frac{1}{u}\right)$ $p_1 \in (p_2, \infty)$	$u - \frac{1}{q} < 0$ $p_2 - p_1 < 0$	stable sink

4. Results. Simulations produced a series of 27 total graphs illustrating the important aspects of immune cell dynamics and neuroblastoma tumor progression under various treatments. These graphical visualizations revealed critical trends, including the temporal changes in tumor growth and immune cell populations, and demonstrated the relative efficacy of Cyclophosphamide and IL-2 compared to control groups. Notably, the combined therapeutic strategy consistently outperformed single-agent applications, highlighting the potential benefit of multi-drug treatment approaches.

4.1. Parameter selection. The initial conditions and parameters used in the model were informed by the interactions among tumor progression, drug concentration, and patient population, and were tailored to disease stage, with modifications adapted from the literature [15]. Our approach to modeling the immunotherapeutic dynamics of neuroblastoma was grounded in the International Neuroblastoma Risk Group (INRG) staging system [13], which significantly enhanced our ability to compare patient populations in the context of therapeutic interventions.

Table 3: Disease stages derived by the International Neuroblastoma Risk Group (INRG).

Disease Stage	Description
Low Risk	Patients with L1 (localized tumors in one area) or MS (asymptomatic with favorable biology and metastases limited to skin, liver, or bone marrow) are considered low risk. These patients typically require observation, with surgery or chemotherapy only if symptoms arise.
Intermediate Risk	L2 (regional tumors with IDRFs) and MS with unfavorable biology (e.g., diploidy) are classified as intermediate risk. These tumors may need chemotherapy, with surgery recommended if possible.
High Risk	M (distant metastases), MS with MYCN amplification, or L2 in patients over 18 months with unfavorable features are high risk. These patients require aggressive treatment including chemotherapy, surgery, and stem cell therapy.

In this study, we employed a three category system to stratify patient populations into low, intermediate, and high-risk groups based on the tumor stages described in Table 3. This system supported the comparative analyses across trials and informed our initial conditions for the developed mathematical model. By aligning with an internationally accepted risk framework, we enhanced the clinical relevance and reproducibility of our simulations.

For each risk group, an estimated relative initial abundances of tumor cells, CTLs, and NK cells, was made while paying particular attention to capturing the relative population sizes as shown in Table 5. These immune profiles enabled accurate simulations of treatment outcomes under varying immunological baselines and allowed for exploration on how the immune system can be influence therapeutic responses.

The low-risk population was initially characterized by a low tumor cell count and a highly active immune response, where NK cells offered immediate defense to tumor cells, whilst CTLs provided a targeted and long-term defense compared to NK cells. In the intermediate-risk population, the tumor cell count is higher, showing a increasingly significant role for CTLs in long-term immune responses. Though NK cells served initially as the first line of defense, the increased tumor burden necessitated a coordinated immune response, with CTLs becoming increasingly critical for targeting and eliminating the growing tumor cells. In high-risk patient population, the tumor cell count is elevated, and the immune system faces greater challenges. While NK cells provided an early line of defense and gradually declined over time, CTLs proved to be essential for long-term tumor control. CTLs ability to recognize specific antigens and undergo clonal expansion enabled a sustained immune response against rapidly proliferating tumor cells.

Table 4: Tumor-pharmacology parameter values.

Parameter	Value
NK cell growth rate (a_1)	0.111
NK cell death rate due to natural death (a_2)	0.0412
Carrying capacity coefficient for NK cell population (b)	1.02e-09
Natural tumor cell growth rate (c)	0.514
Carrying capacity coefficient for tumor cell population (d)	1.02e-09
Rate of NK cell death due to tumor interaction (α_1)	1e-07
Rate of NK-induced tumor death (α_2)	3.23e-07
Rate of CTL-cell death due to tumor interaction (β_1)	3.422e-10
Rate of CTL-induced tumor death (β_2)	0.01245
CTL cell death rate due to natural death (μ)	0.02
Rate of NK-lysed tumor cell debris activation of CTLs (r_1)	2.908e-11
Rate constant of Cyclophosphamide-mediated tumor death (k_c)	0.9
Rate constant of IL-2-mediated stimulation (k_i)	5e+04
Half-life of IL-2 (h_i)	5
Half-life of Cyclophosphamide (h_c)	537
Dose of IL-2 (I_0)	variable
Dose of Cyclophosphamide (C_0)	variable

The model parameters listed in Table 1 were selected to reflect the biological processes driving neuroblastoma progression, immune system interactions, and the therapeutic effects of IL-2 and Cyclophosphamide. NK cell populations were regulated by intrinsic growth (a_1), death (a_2), and a carrying capacity constraint (b), while tumor-induced cytotoxicity was governed by the interaction rate (α_1). CTL dynamics were shaped by activation through NK-lysed tumor byproducts (r_1), natural cell death (μ), and tumor-induced depletion (β_1). Tumor proliferation was defined by the growth rate (c) and the carrying capacity (d), with immune-mediated reduction captured by NK and CTL-mediated lysis (α_2, β_2).

Table 5: Initial cell counts for low, intermediate, and high risk scenarios.

Cell Type	Risk		
	Low	Intermediate	High
$N(0)$	10^5	10^5	10^4
$L(0)$	20	20	20
$T(0)$	8×10^5	10^7	10^7

Drug-related parameters included the rate of IL-2 stimulation of NK cells (k_i) and the rate of Cyclophosphamide induced tumor reduction (k_c), both of which play important roles in modulating immune response and tumor growth in neuroblastoma. Their concentrations were modeled using first-order exponential decay based on the respective drug half-lives (h_i, h_c), capturing the transient nature of these agents in systemic circulation. Initial dosages of IL-2 (I_0) and Cyclophosphamide (C_0) define the dosing schedule for treatment simulations shown in Table 6.

4.1.1. Pharmacological schedules. Dosing schedules for Cyclophosphamide and Interleukin-2 (IL-2) were differentiated by treatment intensity (low-dose and high-dose) and were divided into initial and recurring administrations. For Cyclophosphamide, low-dose treatment involved an initial dose of 2.5 mg/kg followed by recurring doses of 2 mg/kg every 24 hours. High-dose treatment began with an initial dose of 30 mg/kg, with recurring doses of 25 mg/kg administered at 24-hour intervals [6]. IL-2 was administered on a fixed 24-hour cycle. Low-dose schedules involved an initial and recurring dose of 3×10^6 units, while high-dose schedules used 6×10^6 units per dose on the same interval [16].

Table 6: Dosing schedules for Cyclophosphamide and Interleukin-2.

Drug	Dosage	Initial	Recurring
Cyclophosphamide	Low	2.5 mg/kg	2 mg/kg
	High	30 mg/kg	25 mg/kg
IL-2	Low	–	3×10^6 units
	High	–	6×10^6 units

4.1.2. Therapeutic agent selection. Two therapeutic agents were selected for modeling neuroblastoma treatment: Cyclophosphamide and IL-2. These drugs were chosen for their complementary mechanisms in which they affect cellular population [6, 19]. Cyclophosphamide acts through direct tumor cell cytotoxicity, whilst IL-2 enhances immune system activation. By incorporating both agents into our model, we aimed to quantify how chemotherapy induced tumor cell death and immune mediated tumor suppression independently and synergistically. This approach allowed for the exploration of direct cytotoxic effects and immune system activation across different stages of patient diseases.

Cyclophosphamide, a chemotherapy drug, directly targets tumor cells by slowing the rate at which they proliferate and inducing apoptosis. Chemically, the drug alkylates DNA, leading to the formation of cross links that interfere with replication and trigger cell death, in particular with rapidly dividing cells. Beyond its direct cytotoxicity, Cyclophosphamide controls the tumor microenvironment by suppressing immune responses [6]. Despite its effects, its potent ability to reduce tumor burden makes it a cornerstone in neuroblastoma treatment in modern medicine.

IL-2, an immune-modulating cytokine, plays a critical role in activation of NK cells, which are essential for the innate immune response against tumor cell development. IL-2 binds to receptors in NK cells, promoting proliferation, activation, and cytotoxicity. Activated NK cells then directly eliminate tumor cells by releasing

perforin and granzymes, inducing apoptosis [19]. IL-2 enhances the expression of activating receptors in NK cells, improving their ability to recognize and target tumor cells, especially early on in the immune defense. In neuroblastoma treatment, this immune activation supports a shift toward a tumor-targeting immune environment [19].

4.1.3. Simulation of trial scenario. The model was first tested with a combination of parameters that the stability analysis showed resulting in a stable system.

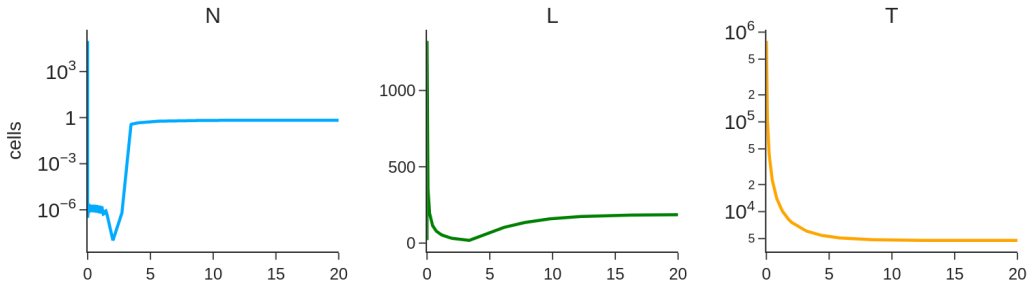

Fig. 2: Numerical simulation results for stable parameters.

In Figure 2, NK and CTL populations showed an initial decline but began recovering by day 5, with NK cell resurgence supporting CTL stabilization. By day 15, both populations reached steady-state levels. While insufficient to eliminate the tumor, immune activity maintained the tumor burden below 10^4 cells. The following section introduces dosing schedules from Table 6 to further explore treatment outcomes.

4.2. Simulation of treatment strategies. Our analysis assessed various combinations of immunotherapy and chemotherapy across three distinct neuroblastoma patient populations stratified by risk level. Simulations were conducted to evaluate how treatment intensity and type influenced therapeutic outcomes within each group.

Table 7: Simulation matrix showing 9 applied treatments across three patient populations.

Risk	Cyclophosphamide Dose	IL-2 Dose		
		None	Low	High
Low	None	Low Risk No Cyclophosphamide No IL-2	Low Risk No Cyclophosphamide Low IL-2	Low Risk No Cyclophosphamide High IL-2
	Low	Low Risk Low Cyclophosphamide No IL-2	Low Risk Low Cyclophosphamide Low IL-2	Low Risk Low Cyclophosphamide High IL-2
	High	Low Risk High Cyclophosphamide No IL-2	Low Risk High Cyclophosphamide Low IL-2	Low Risk High Cyclophosphamide High IL-2
Intermediate	None	Intermediate Risk No Cyclophosphamide No IL-2	Intermediate Risk No Cyclophosphamide Low IL-2	Intermediate Risk No Cyclophosphamide High IL-2
	Low	Intermediate Risk Low Cyclophosphamide No IL-2	Intermediate Risk Low Cyclophosphamide Low IL-2	Intermediate Risk Low Cyclophosphamide High IL-2
	High	Intermediate Risk High Cyclophosphamide No IL-2	Intermediate Risk High Cyclophosphamide Low IL-2	Intermediate Risk High Cyclophosphamide High IL-2
High	None	High Risk No Cyclophosphamide No IL-2	High Risk No Cyclophosphamide Low IL-2	High Risk No Cyclophosphamide High IL-2
	Low	High Risk Low Cyclophosphamide No IL-2	High Risk Low Cyclophosphamide Low IL-2	High Risk Low Cyclophosphamide High IL-2
	High	High Risk High Cyclophosphamide No IL-2	High Risk High Cyclophosphamide Low IL-2	High Risk High Cyclophosphamide High IL-2

4.2.1. Low Risk. Low-risk simulations began with relatively small tumor populations and exhibited a partially functional immune system.

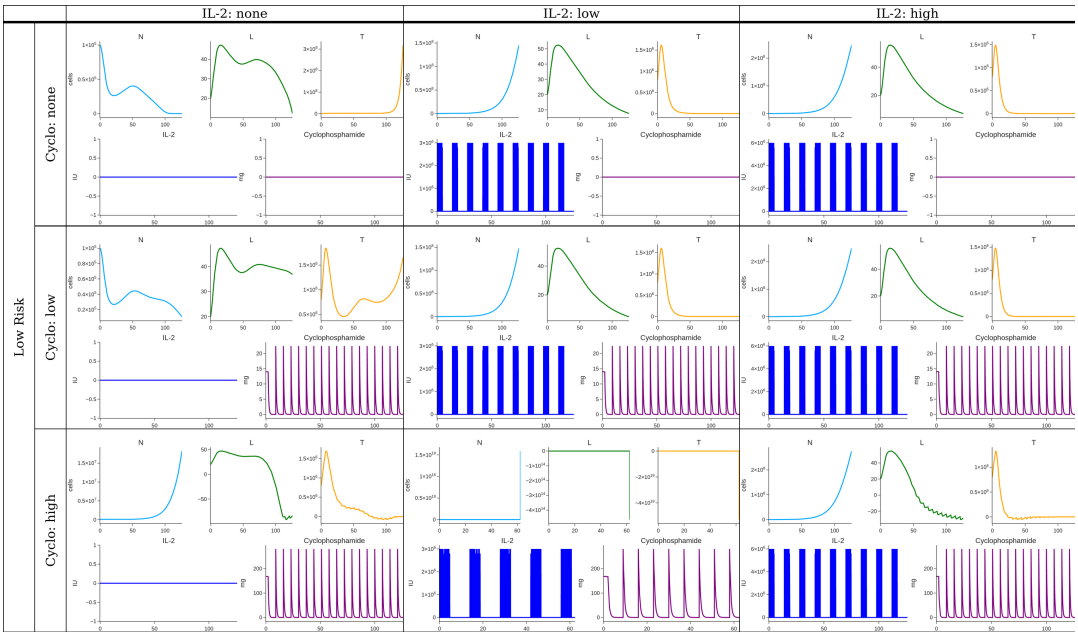

Fig. 3: Low-risk simulation results.

The results in Fig. 3 showed either high doses of Cyclophosphamide or low doses of Interleukin-2 were necessary to overcome proliferating tumor cells. Low doses of Cyclophosphamide temporarily decreased the amount of tumor cells, however as the tumor continued to grow it eventually outpaced the impact of Cyclophosphamide. Interleukin-2, was much more effective at suppressing tumor growth by increasing NK cell production with a low dose showing to be sufficient. Combinations of interleukin-2 and high doses of Cyclophosphamide with these initial conditions resulted in numerical instability as tumor cell counts becomes negative.

4.2.2. Intermediate-Risk. Intermediate-risk simulations were initialized with a higher tumor burden and a moderately suppressed immune response.

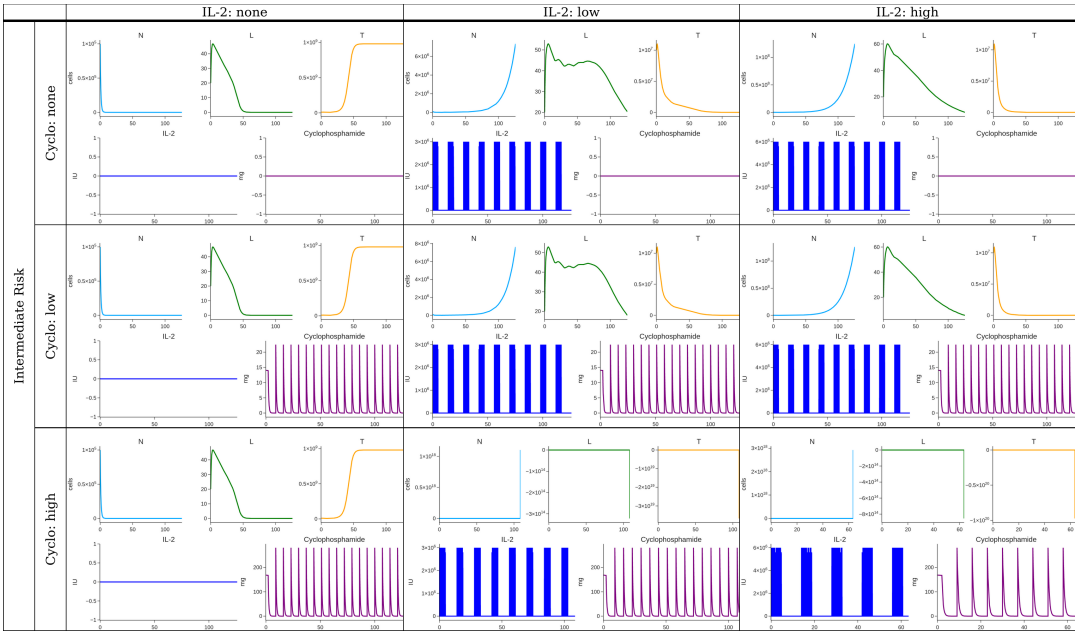

Fig. 4: Intermediate-risk simulation results.

The results show in Fig. 4 that administering Interleukin-2 was necessary to overcome higher tumor burdens. Both low and high doses of Cyclophosphamide were insufficient at this stage. Simulations with interleukin-2 and high doses of Cyclophosphamide were administered and were numerically unstable as the tumor cell count eventually became negative.

4.2.3. High-Risk. High-risk simulations were characterized by aggressive tumor growth and severely compromised immune cell populations.

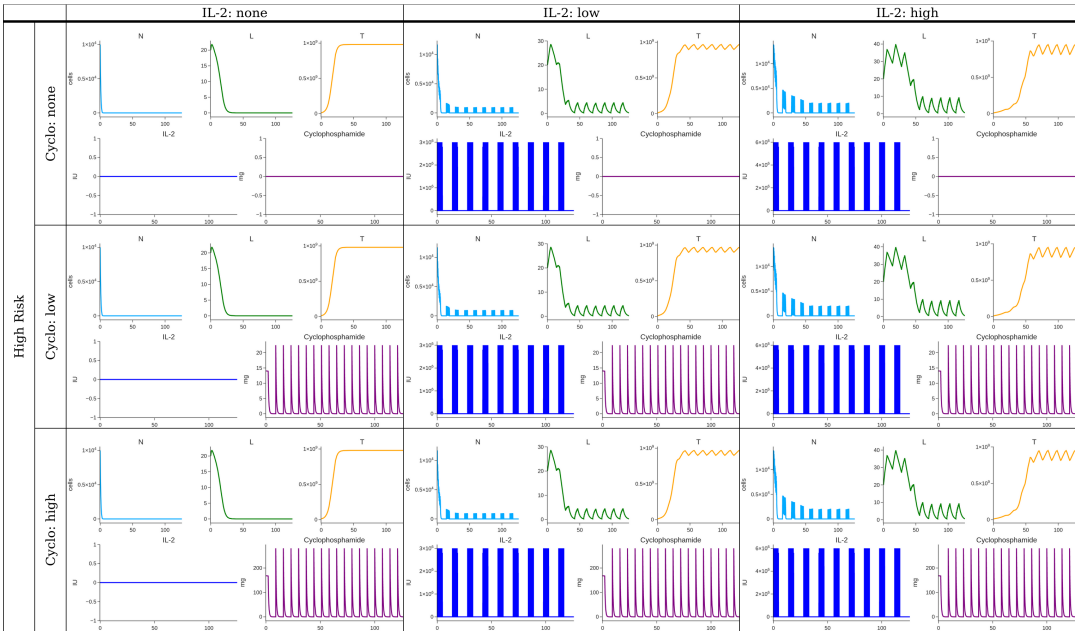

Fig. 5: High-risk simulation results.

The results show in Fig. 5 showed that no FDA approved combination of interleukin-2 and Cyclophosphamide could suppress tumor cells in high risk conditions. Administering either low or high doses of Cyclophosphamide result in no perceivable changes. Administering either low or high doses of interleukin-2 results in bursts of immune activity which quickly became overwhelmed by tumor cells.

5. Conclusion. This study examined the interactions between tumor cells, immune responses, and therapeutic agents in neuroblastoma using a system of coupled first-order ordinary differential equations. Our results emphasized and showed the crucial role NK cells and CTLs have in suppressing tumor growth and that both Interleukin-2 and Cyclophosphamide enhanced immune-mediated tumor elimination in low-risk conditions. In intermediate-risk scenarios, IL-2 was found to be an effective therapeutic strategy. However, for high-risk cases, no effective treatment combinations using FDA-approved dosing schedules of IL-2 and Cyclophosphamide were identified within the scope of this study. Nonetheless, the presented model is adaptable for future investigations incorporating alternative drugs or treatment strategies to explore additional therapeutic options.

By integrating immunotherapeutic and chemotherapeutic agents, our model highlighted the potential of combining drug therapies, providing valuable insights for treatment optimization strategies for neuroblastoma pateints.

Data availability. Code and data used in this study is available on GitHub at: https://github.com/JGarza189/neuroblastoma-2025.

Acknowledgments. Our team extends sincere gratitude to Dr. BV Shankara Narayana Rao for her guidance and support throughout the project. Additionally, we would like to thank the Texas A&M High Performance Research Computing Group for portions of this research which were conducted with the advanced computing resources provided by Texas A&M High Performance Research Computing.

References

[1] J. Anderson, R. G. Majzner, and P. M. Sondel. "Immunotherapy of neuroblastoma: Facts and hopes". In: *Clinical Cancer Research* 28.15 (2022), pp. 3196–3206.

[2] R. J. Arceci. "The International Neuroblastoma Risk Group (INRG) classification system: An INRG task force report". In: *Yearbook of Oncology* 2009 (2009), pp. 162–163.

[3] N. Bellomo, L. Preziosi, and G. Forni. "Tumor immune system interactions: The kinetic cellular theory". In: *A Survey of Models for Tumor-Immune System Dynamics*. 1997, pp. 135–186.

[4] S. Benzekry et al. "Classical Mathematical Models for Description and Prediction of Experimental Tumor Growth". In: *PLoS Computational Biology* 10.8 (2014), e1003800.

[5] F. Berthold and B. Hero. "Neuroblastoma". In: *Drugs* 59.6 (2000), pp. 1261–1277.

[6] A. Emadi, R. J. Jones, and R. A. Brodsky. "Cyclophosphamide and cancer: Golden Anniversary". In: *Nature Reviews Clinical Oncology* 6.11 (2009), pp. 638–647.

[7] Sinisa Franjić. "Neuroblastoma is a Type of Cancer that mainly Occurs in Young Children". In: *R, R, RJ of Cancer & Oncology* 2.3 (2024), pp. 01–04.

[8] G. S. Getz. "Bridging the innate and adaptive immune systems". In: *Journal of Lipid Research* 46.4 (2005), pp. 619–622.

[9] M. E. Katt et al. "In vitro tumor models: Advantages, disadvantages, variables, and selecting the right platform". In: *Frontiers in Bioengineering and Biotechnology* 4 (2016), p. 12.

[10] V. A. Kuznetsov et al. "Nonlinear dynamics of immunogenic tumors: Parameter estimation and global bifurcation analysis". In: *Bulletin of Mathematical Biology* 56.2 (1994), pp. 295–321.

[11] D. Loose and C. Van de Wiele. "The immune system and cancer". In: *Cancer Biotherapy and Radiopharmaceuticals* 24.3 (2009), pp. 369–376.

[12] C. Ménard et al. "Cancer chemotherapy: Not only a direct cytotoxic effect, but also an adjuvant for antitumor immunity". In: *Cancer Immunology, Immunotherapy* 57.11 (2008), pp. 1579–1587.

[13] S. Mueller and K. K. Matthay. "Neuroblastoma: Biology and staging". In: *Current Oncology Reports* 11.6 (2009), pp. 431–438.

[14] A. Padder et al. "Dynamical analysis of generalized tumor model with Caputo fractional-order derivative". In: *Fractal and Fractional* 7.3 (2023), p. 258.

[15] L. de Pillis et al. "Mathematical model creation for cancer chemo-immunotherapy". In: *Computational and Mathematical Methods in Medicine* 10.3 (2008), pp. 165–184.

[16] J. G. Pressey et al. "In vivo expansion and activation of 3b33b4 T cells as immunotherapy for refractory neuroblastoma". In: *Medicine* 95.39 (2016).

[17] V. Quaranta et al. "Mathematical modeling of cancer: The future of prognosis and treatment". In: *Clinica Chimica Acta* 357.2 (2005), pp. 173–179.

[18] D. H. Raulet. "Interplay of natural killer cells and their receptors with the adaptive immune response". In: *Nature Immunology* 5.10 (2004), pp. 996–1002.

[19] A. Rossi et al. "Lysis of neuroblastoma cell lines by human natural killer cells activated by interleukin-2 and interleukin-12". In: *Blood* 83.5 (1994).

[20] N. K. Roy et al. "Cancer — an overview and molecular alterations in cancer". In: *Fusion Genes and Cancer* (2017), pp. 1–15.

[21] V. Smith and J. Foster. "High-risk neuroblastoma treatment review". In: *Children* 5.9 (2018), p. 114.

[22] Ge Song, Tianhai Tian, and Xinan Zhang. "A mathematical model of cell-mediated immune response to tumor". In: *Mathematical Biosciences and Engineering* 18.1 (2021), pp. 373–385.

[23] Ge Song et al. "Mathematical modeling and analysis of tumor chemotherapy". In: *Symmetry* 14.4 (2022).